Received: 10 August 2016 | Revised: 14 October 2016 | Accepted: 7 December 2016

DOI 10.1002/cm.21350

RESEARCH ARTICLE

Dynamics of the sealing zone in cultured osteoclasts

Sarit Batsir | **Benjamin Geiger** | **Zvi Kam**

Department of Molecular Cell Biology, Weizmann Institute of Science, Rehovot, Israel

Correspondence
Benjamin Geiger, Department of Molecular Cell Biology, Weizmann Institute of Science, Rehovot 7610001, Israel.
Email: benny.geiger@weizmann.ac.il

Funding information
European Union's Seventh Framework Programme (FP7/2007-2013), Grant/Award Number: n 258068

Abstract

Bone resorption by osteoclasts (OCs) depends on the formation and stability of the sealing zone (SZ), a peripheral belt of actin and integrin-based podosomes. Recent studies demonstrated that the SZ is a highly dynamic structure, undergoing cycles of assembly and disassembly. In this study, we explored the mechanisms underlying the regulation of SZ stability and reorganization in OCs cultured on glass slides, and forming an SZ-like podosome belt (SZL). By monitoring this belt in cultured RAW264.7 cells expressing GFP-tagged actin, we show here that SZL stability is usually locally regulated, and its dissociation, occurring mostly in concave segments, is manifested in the loss of both podosome coherence, and actin belt continuity. Double labeling of cells for actin and tubulin indicated that microtubules (MTs) are mostly confined by the inner aspect of the stable SZL-associated actin belt. However, in unstable regions of the SZL, MTs tend to extend radially, across the SZL, toward the cell edge. Disruption of MTs by nocodazole induces SZ disassembly, without affecting individual podosome stability. Inspection of the MT network indicates that it is enriched along stable SZL regions, while bypassing disorganized regions. These results suggest that the SZL is stabilized by MTs flanking its inner aspect, while disruption or misalignment of MTs leads to SZL destabilization. We further demonstrate that the MT-associated protein dynamin2 is involved in the regulation of SZL stability, and dynamin2 knockdown or inactivation cause SZL destabilization.

KEYWORDS
dynamin2, osteoclasts, podosomes, RAW cells, sealing zone-like podosome belt

1 | INTRODUCTION

Osteoclasts (OCs) are bone-degrading, multinucleated cells derived from the monocytic cell lineage (Mulari, Vaaraniemi, & Väänänen, 2003; Väänänen et al., 2000). Mature OCs adhere to bone surfaces by forming a contiguous adhesion belt, known as the sealing zone (SZ), which anchors the OCs to the bone surface and delimits the so-called "resorption lacuna," (Lakkakorpi & Väänänen, 1996). The ruffled border facing the bone substrate is the active resorption organelle through which protons and proteolytic enzymes are secreted into the resorption lacuna, and bone degradation products are endocytosed and removed (Mulari et al., 2003).

The SZ belt is composed of a closely packed array of actin-rich adhesion structures, namely podosomes, that form a tight diffusion barrier, separating the resorption lacuna from the surrounding bone surface, thus enabling OCs to remodel bone effectively, and with high spatial precision (Lakkakorpi, Helfrich, Horton, & Väänänen, 1993; Pfaff & Jurdic, 2001; Väänänen & Horton, 1995). Evidently, the regulation of bone resorption is of great physiological importance, given that enhanced or decreased osteoclastic activity leads to the development of pathological states such as osteoporosis and osteopetrosis, respectively (Hagel-Bradway & Dziak, 1989; Manolagas, 2000; Marks, 1987).

Recent studies have shown that the formation of a functional resorptive apparatus in OCs is regulated at different molecular and cellular levels (for review, see Boyce, 2013; Destaing, Petropoulos, & Albiges-Rizo, 2014). These include the stimulation of osteoclastogenesis by Receptor Activator of Nuclear Factor Kappa-B Ligand (RANKL), the fusion of precursor cells into multicellular OCs (Soysa, Alles, Aoki,

Monitoring Editor: George Bloom

& Ohya, 2012), and the formation of podosomes, and their assembly into a functional SZ (Georgess, Machuca-Gayet, Blangy, & Jurdic, 2014). In this study, we focused primarily on the cytoskeletal mechanisms that regulate SZL formation and stability and, in particular, on the interplay between the actin cytoskeleton and microtubules (MTs).

Bone constitutes the physiological substrate for OCs. A comparison of OCs cultured on various surfaces found the architecture of the basic adhesion unit (i.e., the podosome) to be similar in cells that grow on glass, on calcite, and on bone, although differences in actin assembly dynamics were reported (e.g., Salter, Destaing, Bard, Eichert, & Jurdic, 2004). Further assembly of podosomal superstructures is also surface-sensitive. The fluorescence intensity of podosome-associated actin in SZs formed on bone and calcite is higher than those that are formed on glass, and the SZs that are formed on calcite and bone are about twice as wide as the SZ-like (SZL) structures that are formed on glass. The reasons for these differences are not clear. SZs in OCs cultured on glass display faster dynamics (on a scale of minutes), while on calcite, small rings merge to form stable SZL structures over a period of several hours; furthermore, their stability may depend on substrate topology.

Despite these differences, accumulating evidence suggests that the basic structure of the SZ, and its cellular controls, are mostly shared between glass and bone. Moreover, bone is not essential for OC activation and function. We successfully utilized glass as a model system for our dynamical studies, since compared with bone, glass slides provide conditions for improved optical imaging.

The SZ is primarily an actin-based structure composed of podosomes interconnected by a robust F-actin belt (Teitelbaum, 2011). Individual podosomes are surrounded by ring-like adhesion proteins with a diameter of $\sim$1 μm (Luxenburg, Addadi, & Geiger, 2006), containing integrins (mainly $\alpha_V\beta_3$) and other adhesome components, and a cylindrical F-actin "core" bundle, running largely perpendicular to the membrane (Destaing, Saltel, Géminard, Jurdic, & Bard, 2003). In podosome super-structures such as the SZ, dense networks of actin filaments run between the actin cores of neighboring podosomes, keeping them close to one another and, apparently, mechanically integrated (Geblinger, Geiger, & Addadi, 2009).

MT are known to target both the focal adhesions anchoring cells to their substrate (Kaverina, Krylyshkina, & Small, 1999), and podosomes (Evans, Correia, Krasavina, Watson, & Matsudaira, 2003; Kopp et al., 2006). Specifically, the integrity of the MT network was shown to be crucial for podosome organization (Destaing et al., 2003; Jurdic, Saltel, Chabadel, & Destaing, 2006); furthermore, depolymerization of MTs by nocodazole treatment was seen to destabilize individual podosomes (Destaing et al., 2005) and to disrupt the SZ-associated podosome belt in OCs (Destaing et al., 2003). While these effects are well-documented, the molecular and cellular mechanisms whereby MTs affect podosome recruitment into the SZ and control its assembly, dynamics, and stability are still poorly understood.

In this study, we used quantitative live-cell imaging to explore the morphological and molecular dynamic features of stable and unstable regions of the SZL. In doing so, we demonstrate that local instability is commonly confined to concave segments of this belt, which display rapid displacement of podosome sites of assembly and relatively low local actin intensities, and suggest the presence of shorter podosome cores, and fewer interpodosomal actin filaments. Analysis of time-lapse movies of OCs expressing fluorescently tagged actin indicated that cycles of stability and instability in specific regions along the SZL are not synchronized, implying regional, rather than global, control of its dynamics.

We further show that when MTs are disrupted by nocodazole, podosome compaction within the SZL is radically reduced. Their localization is initially confined to the vicinity of the SZL, yet over time, they progressively become scattered throughout the cell. This response to nocodazole suggests that MTs might be involved in the regulation of podosome compaction in the SZL. Localization of the relative distributions of F-actin and tubulin in cultured OCs indicated that in stable regions of the SZL, MTs reach out toward the actin belt, while in unstable regions; MTs usually extend radially, crossing the residual actin belt toward the cell periphery. Searching for the mechanism underlying the cross-talk between the microtubular system and the actin-rich SZL, we noticed that dynamin1 and 2 in mouse embryonic fibroblasts associate with podosomes and affect their function, although individual podosomes do not disappear (Destaing et al., 2013). In OCs, we found that dynamin2 inactivation or knockdown lead to dramatic SZL destabilization and podosome dispersion, in a pattern similar to MT disruption effect. The implications of these findings on the regulation of podosome functions are discussed.

2 | RESULTS

2.1 | The stability of the SZ is affected by its curvature

The stability of the SZL was studied by time-lapse, microscopy-based imaging of RAW246.7 OCs expressing GFP-tagged actin. Examination of the resulting movies indicated that convex SZL contours (those bending toward the cell periphery) are mostly stable, while concave regions (bending toward the center of the SZL) are unstable, manifested by fast displacement or complete disassembly of the SZL. To quantify these changes in the morphological and molecular features of SZL dynamics, we manually marked the SZL path in each frame of the time-lapse movie. Quantitative analysis was performed for 4 movies, and visual inspection of 10 movies confirm the following conclusions.

Four time-dependent variables were quantified along the path: actin intensity, SZL displacement velocity, local curvature, and spatial intensity variance (see Figure 1, legend). These quantities are color-coded along the drawn SZL (four slightly displaced track lines are shown for the four parameters in each time frame; Figure 1a).

To display the time dependence of the four features all at once, kymographs were built by stacking horizontal straightened strips of the color-coded paths as a function of time (Figure 1b). They point to a strong correlation between regions displaying a concave SZL, and high curvature and fast displacements. These regions also display lower local actin intensities, flanked by higher actin intensities in stable neighboring regions. Thus, low local actin intensities are correlated with concave regions with high displacement velocities and high variance, characterizing unstable SZL regions in which individual podosomes are

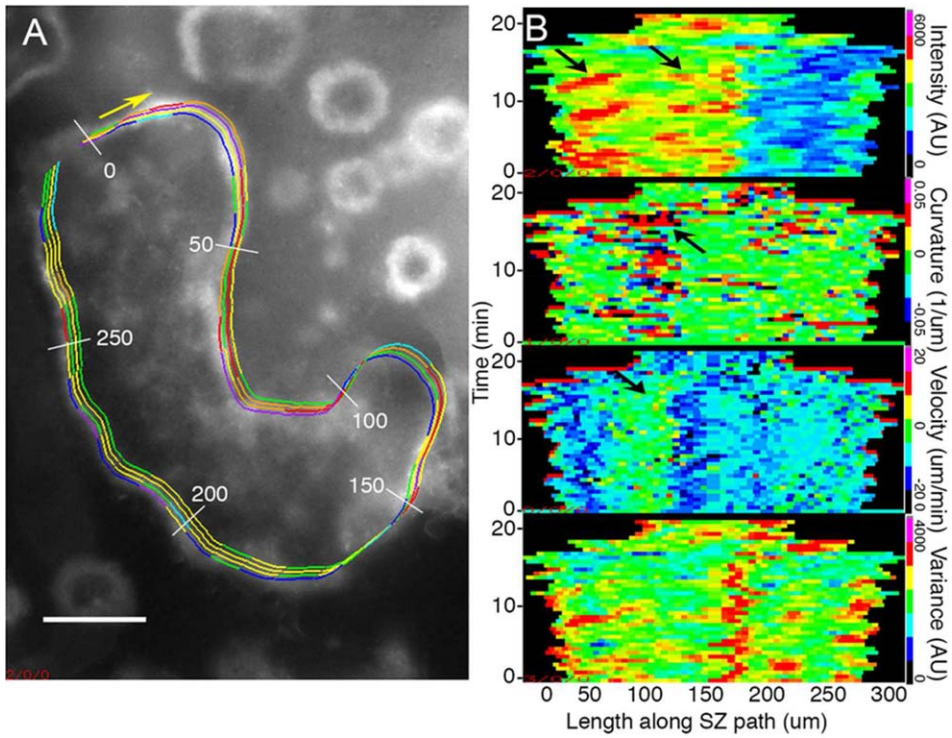

FIGURE 1 Assessment of SZL dynamics. (a) Actin-GFP-tagged OCs were fluorescently imaged at a rate of one frame every 30 s. Images of the SZL-associated actin were outlined manually, frame-by-frame, in four movies, one presented here, and linearized (start point indicated by the yellow arrow). The path was then divided into 50 pixel-long segments; for each segment, four properties were quantified: (1) *Average intensity* (in 5 pixel-wide strips taken along the segment); (2) *Curvature* (inverse radius of fitted circle, defined as positive for the convex curve with respect to the cell center); (3) *velocity* (translocation of the SZL segment center from one timeframe to the next (displacement away from the cell center was defined as positive), and (4) pixel-by-pixel *variance* within the strip area (contiguous belts yield low variance, whereas clusters of individual podosomes yield high variance). Variance is calculated as $\mathrm{sqrt}[<(I(x,y)-I_{avg})^2>]/I_{avg;}\ I_{avg}=<I(x,y)>$, where $I(x, y)$ is image intensity at pixel (x,y), and $<>$ marks the averaged variance in the region of interest. The values of these properties are color-coded, and displayed as four slightly shifted belt path outlines. Distances from the start of the path are marked in white numbers along the path. (b) Presentation of the color-coded values along the "straightened" SZL path, stacked as a function of time to display as kymographs. Each of the four horizontal strips represents the quantified properties along the path. The kymographs illustrate regions with a strong correlation between high belt concave curvature and fast belt velocity. These regions also correlate with low actin intensity and high variance, and are usually flanked by high actin intensity regions with low variance; see black arrows. Scale bar: 25 μm.To quantify this data, we calculated Pearson correlation coefficients between the 6 pairs of the 4 measured curves, averaged on the whole path and over 40 time frames for 4 movies. The correlation coefficients are averaged on the entire SZL path. Values obtained for selected regions yield higher correlations; Curvature-Velocity: Cor1 = -0.6 ± 0.3; Curvature-Intensity: Cor2 = 0.4 ± 0.2; Velocity-Intensity: Cor3 = -0.3 ± 0.1; Curvature-Variance: Cor4 = 0.3 ± 0.2; Velocity-Variance: Cor5 = 0.2 ± 0.1; Intensity-Variance: Cor6 = -0.2 ± 0.1.

discerned. Due to the high lateral density of podosome cores throughout the SZ, as well as the prominence of interconnecting actin filaments that run between them (Geblinger et al., 2009; Luxenburg, Winograd-Katz, Addadi, & Geiger, 2012), we cannot unequivocally relate the higher actin intensity segments in stable regions of the SZ to longer actin cores, higher density of interconnecting actin filaments, and/or higher density of podosome core packing,

2.2 | Local control of SZ stability

Live monitoring of RAW246.7 OCs expressing GFP-tagged actin indicated that the temporal variations of actin intensity in different regions along the same SZL display cyclic changes over a period of minutes (for the cell shown in Figure 1, see Figure 2a). Interestingly, these local assembly disassembly cycles are not synchronized throughout the SZL, indicating that control of SZL stability is local or regional, rather than global. To test whether specific regions along the SZL display greater long-term stability than others, we subjected the time-dependent actin fluorescence intensity $I(t)$ for various ~20 micron regions along the SZL, to temporal autocorrelation analysis. The autocorrelation functions (Figure 2b) for the various regions (Figure 2c) were practically identical, indicating that stability (at least on glass) is not maintained as a local property. The very small shoulders in the autocorrelation function, resulting from the cyclic changes in local actin intensity, imply wide variability in the cycle periods. These analyses were repeated for five movies.

2.3 | The involvement of MTs in the stability of the SZ

Another cytoskeletal component that is known to be involved in SZL stability is the MT network. To explore how actin and MTs collaborate

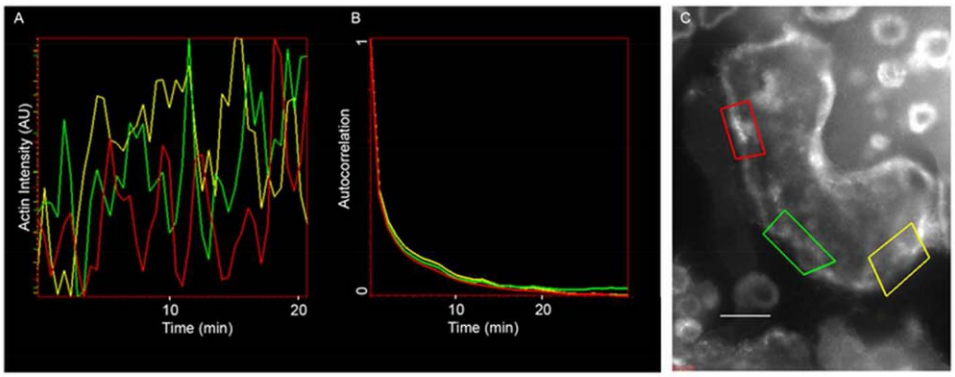

FIGURE 2 Quantitative analysis of SZL features. (a) Segments (20 μm-long) along the movies of SZL paths were outlined by polygons, and total actin intensity was quantified as a function of time. Total intensities include both distinct podosomes and "cloud" actin contributions. About 5 min-long cycles of increasing and decreasing intensity are shown in three such regions for the cell shown in Figure 1; see red, yellow, and green polygons in (c). Lack of synchronization between these cyclic behaviors in the various regions, visually apparent in all movies we acquired, suggests local, rather than global, regulation of SZL stability. (b) Autocorrelations (averaged over more than four assembly disassembly cycles) for the three curves shown in Figure 2a, indicating that they are essentially identical, and implying a lack of long-term instability in specific regions along the SZL. Kolmogorov-Smirnov comparison p-value = 0.996. Although the curve is not strictly a single exponent, an exponential fit for the fast region yields $\tau = 1 \pm 0.2$ min ($n = 10$).

in the assembly and disassembly of the SZL, we treated mature OCs with the MT inhibitor nocodazole, and monitored the effect of this treatment on SZL stability. As shown in Figure 3a–c, following OC exposure to the drug for 20 min or more, compact SZL disappeared; however, individual podosomes persisted, dispersing and undergoing assembly and disassembly throughout the cell. It is noteworthy that in untreated cells, podosome assembly is confined primarily to the vicinity of the SZL. As shown in Figure 3d, podosomes were mostly detected within ±4 μm of the cell's edge, prior to addition of the drug. Following nocodazole addition, a gradual increase in the distance between newly assembled podosomes and the disassembling SZL was detected, with no significant change in distance between isolated podosomes. We also tested OCs treated with taxol, but OCs SZL response to taxol was highly variable between cells and made the analysis less clear-cut as with nocodazole.

2.4 | Distinct organization of MTs flanking stable and unstable SZ regions

Three-dimensional imaging of OCs expressing both fluorescently tagged actin (GFP) and the MT-associated protein Ensconsin (mCherry; Bulinski, Odde, Howell, Salmon, & Waterman-Storer, 2001) pointed to distinct differences in the organization of MTs located in the vicinity of stable regions, and those flanking unstable regions of the SZL belt (Figure 4). Specifically, as observed in 10 movies, the MT network appears halted by the central aspect of stable regions of the belt, while it readily crosses

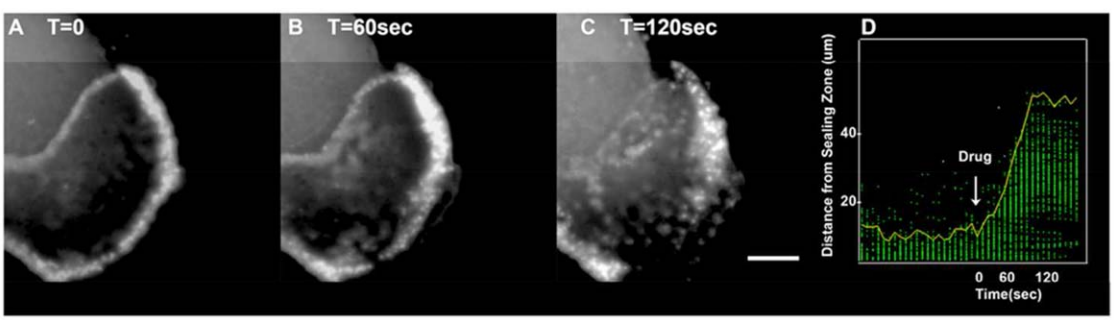

FIGURE 3 Nocodazole treatment inhibits podosome compaction in the SZL. Time-lapse movies of actin-GFP-tagged OCs were acquired at a rate of one frame every 30 s. Following 10 min of recording, 5 μM of nocodazole was added to the cells. (a) SZL recorded prior to nocodazole treatment. (b, c) SZL recorded 1 and 2 min post-nocodazole treatment. (d) Time-dependence analysis of podosome distances from the SZL prior to and during nocodazole treatment. Green dots correspond to podosome centers; the vertical axis indicates distance from the SZL; the horizontal axis indicates time. The yellow curve represents the time dependence of twice the average podosome distance (enveloping the green dots for visualization). The white arrow indicates the time of nocodazole addition. Average podosome dispersion time measured at 25 μm distance is 1 ± 0.3 min ($n = 4$). The distance between the dispersing podosomes (evaluated by the average of minimal distances to closest neighbor, or the average of minimal distances to their five closest neighbors) does not change significantly, as their numbers increase, and they occupy a wider cell area. Scale bar: 40 μm.

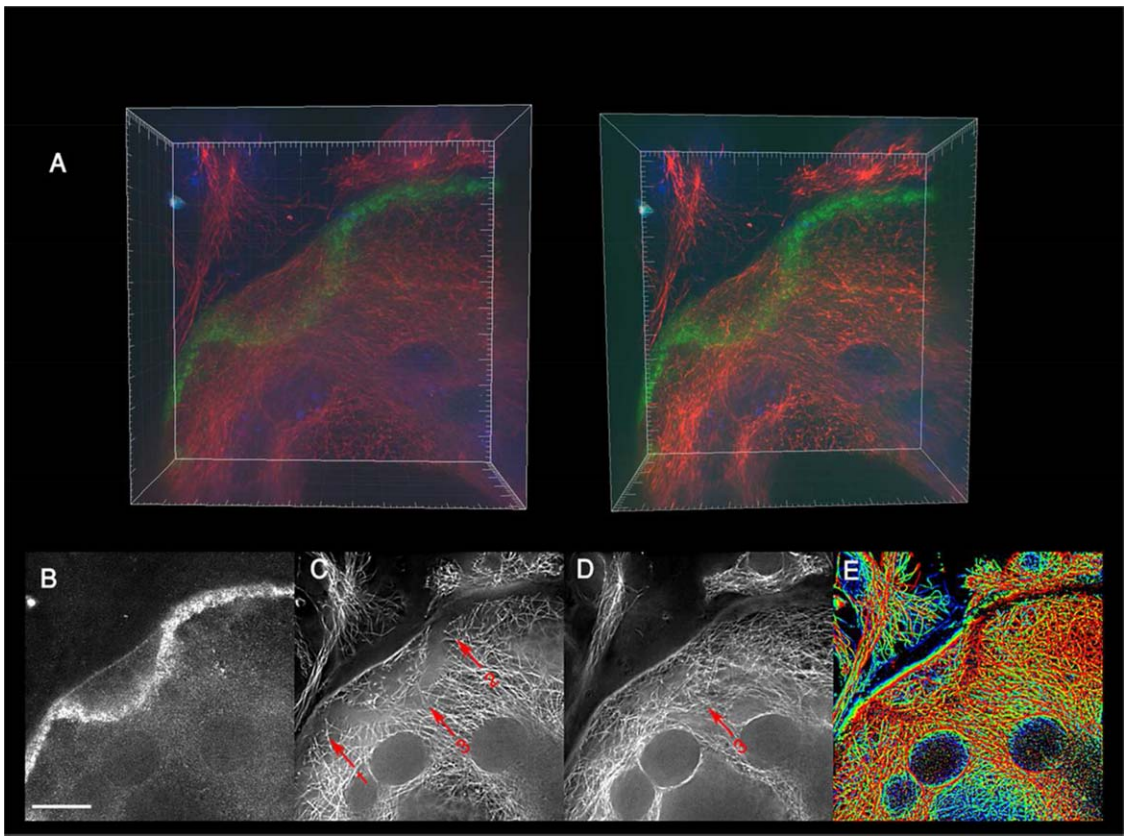

FIGURE 4 3D view of MTs and actin in a mature OC. (a) Focal series of a fully differentiated OC, stained for MT and actin. The 3D series was acquired and subjected to deconvolution and 3D reconstruction by means of Imaris software. (b, c) Two optical sections taken at near-slide level, showing actin and MTs, respectively. MT ends reaching stable SZL regions (Arrows 1-2) can be observed. (d) MTs located 3 μm above the slide surface. MTs run across the unstable region of the SZL toward the cell periphery (Arrow 3). (e) These features are also displayed by the height-coded MT projection image (red indicates high; blue/green indicates low).

unstable SZL regions, and extends beyond the belt toward the cell periphery. Dynamic monitoring of actin and MT in live OCs directly supports this relationship (Supporting Information Movie S1). As shown, MTs typically either stop at the compact actin belt of stable SZL areas, or bend back toward the cell center, whereas MTs approaching unstable SZL regions readily extend across the SZL, and protrude toward the cell periphery.

2.5 | Involvement of dynamin2 in actin and MT interactions, and the regulation of SZ stability

We further hypothesized that there might be an adaptor molecule bridging between the MT system and the actin-containing podosomes, and chose to explore the possibility that dynamin2 is such a molecule, based on reports indicating that it can bind to both MTs and actin (Bruzzaniti et al., 2005; Ochoa et al., 2000). The images presented in Figure 5 show that dynamin2 is distributed around podosome cores, as well as along MTs. About 20% of dynamin2 immunolabeling is found in the vicinity of podosome centers, and 50% of the immunolabeled dots are found on MTs.

To directly test the involvement of dynamin2 in regulating SZL stability, we used dynamin2 mutants. According to previous work (McNiven, Baldassarre, & Buccione, 2004), the proline-rich domain (PRD) plays a central role in dynamin2 targeting to podosomes, since a GFP fusion protein of Dyn2-PRD co-localizes with actin at podosomes, while expression of a PRD deletion mutant of dynamin2 almost completely disrupts podosome assembly. Other Dyn2 domains are critical for actin dynamics, since expression of the dynamin-k44a dominant negative affects actin turnover at podosomes. To test the role of dynamin2 in SZL stability, we overexpressed, in RAW246.7 cells, GFP-tagged dynamin2 (dynamin-2aa), dynamin-ΔPRD (lacking its PRD), and dynamin-k44a, which is mutated in its GTPase domain. We then fixed the samples and stained for MT, actin and dynamin.

In dynamin-2aa-transfected cells, most of the dynamin2 was concentrated along the SZL, which was otherwise coherent and stable. In the dynamin-ΔPRD-expressing cells, the tagged dynamin mostly localized near the SZL; yet the podosomes were scattered throughout the cells, and the SZL appeared fragmented. Expression of the dynamin-k44a dominant negative resulted in small cells, possibly due to disrupted cell fusion, and blocked the formation of the SZL altogether, (Supporting Information Figure S2). Notably, all three transfections had no apparent effect on the organization of MTs that can be clearly observed even in the small cells in S2C. These results support the notion that dynamin is involved in stabilizing the SZL; furthermore, that its GTPase domain is required for this activity.

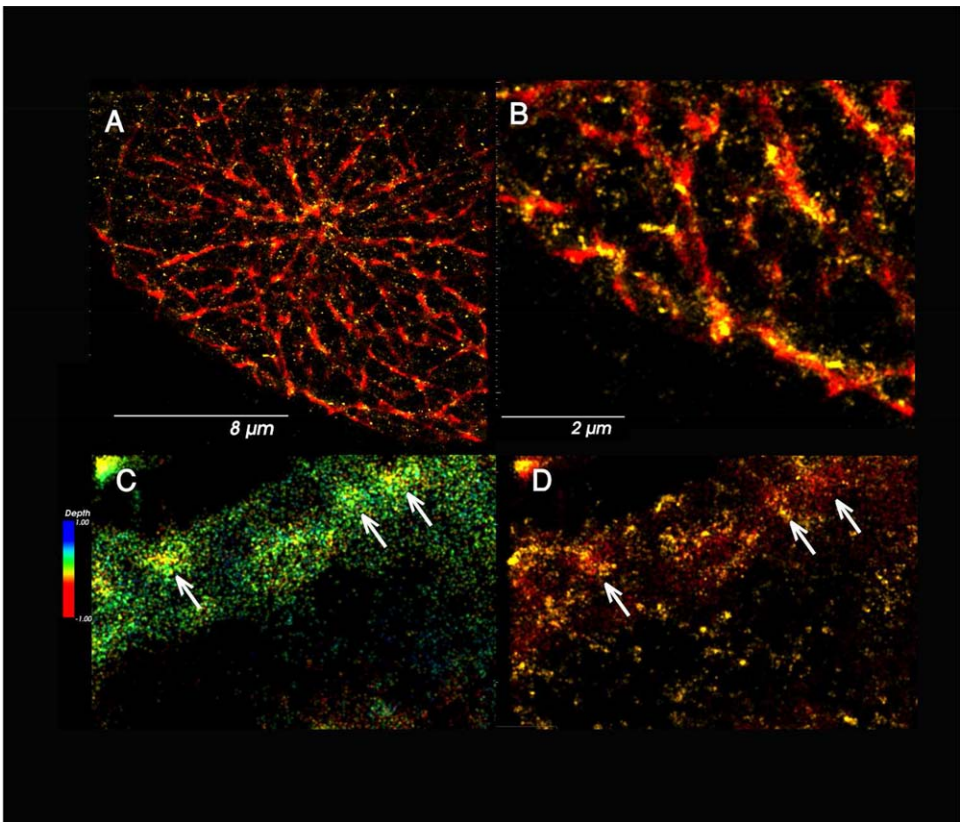

FIGURE 5 MTs, actin and dynamin2 colocalize. Super-resolution images taken from OCs triple-labeled for MT, actin and dynamin2. (a) MTs in red, with dynamin2 in yellow. (b) Zoom-in view, showing that most dynamin2 dots lie near MTs. (c) Actin height color scale. Podosomes (indicated by the arrows) display higher actin loci (yellow). (d) Double labeling for actin (in red) and dynamin2 (in yellow), indicating an abundance of dynamin2 near podosomes. 20% of dynamin2 dots are at a 1 μm distance from podosome centers.

This notion was further substantiated by testing the effect of dyngo-4a, a dynamin2 inhibitor, which binds to the GTPase domain (McCluskey et al., 2013) on OCs expressing GFP-actin and the m-Cherry-tagged MT-associated protein Enconsin. Time-lapse movies were acquired following treatment of OCs with the drug. As shown in Figure 6, OC treatment with Dyngo-4a affected the SZL and podosomes similarly to nocodazole; namely, it scattered podosomes, without grossly affecting their formation. The specimens were fixed at the

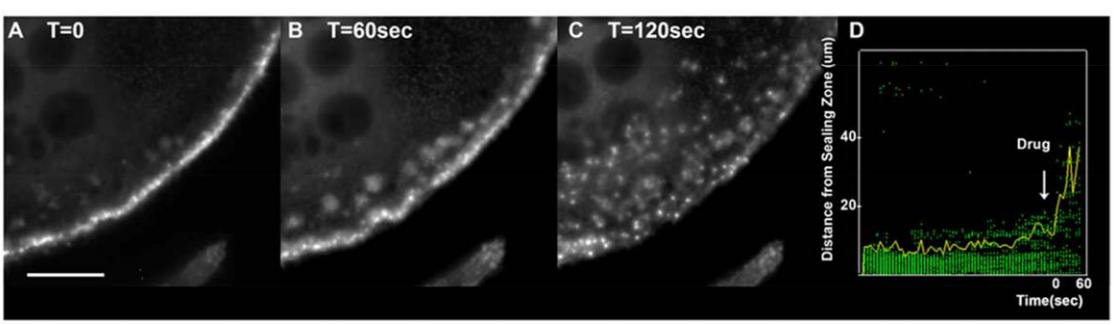

FIGURE 6 Treatment of OCs with the dynamin2 inhibitor Dyngo-4a inhibits podosome compaction in the SZL. A time-lapse movie of actin-GFP-expressing OCs was recorded at 30 s intervals. Following 10 min of recording, 5 μM of Dyngo-4a was added to the samples. (a) Image taken prior to Dyngo-4a treatment. (b, c) Images taken 2 and 4 min after Dyngo-4a treatment. (d) Time-dependence analysis of podosome distances from the SZL prior to and during Dyngo treatment. Green dots indicate podosome centers. Vertical axis—distance from the SZL; horizontal axis corresponds to time. The yellow curve shows the time dependence of twice the average podosome distance (enveloping the green dots for visualization). White arrow indicate time of Dyngo-4a addition. Average podosome dispersion time measured at 25 μm distance is 1 ± 0.4 min ($n = 6$). The distance between the dispersing podosomes (evaluated by the average of minimal distances to closest neighbor, or the average of minimal distances to five closest neighbors) does not change significantly, as their number increases and they occupy a wider cell area. Scale bar: 25 μm.

end of the experiment and labeled for MTs, to confirm that dynamin perturbations act "downstream" of MTs, since dingo disrupts SZL regions, with no effect on the MTs.

The role of dynamin2 in SZL assembly was further substantiated by knocking down dynamin2, using siRNA transfection of differentiated OCs. More than 50% of the cells were transfected, as indicated by low dynamin2 fluorescence. Their images (Supporting Information Figure S3) clearly showed that partial suppression of dynamin2 is sufficient for dispersing the SZL, further supporting the notion that dynamin2 is essential for the compaction and stabilization of the SZL.

3 | DISCUSSION

The functionality of OCs, the primary regulator of bone remodeling, depends on the structural integrity of the main resorption apparatus of these cells, namely the SZ. In this article, we explored the mechanisms underlying the formation, dynamics, and stability of the SZL following the rationale that efficient bone resorption depends on the physical separation of the acidic resorption lacuna from the surrounding environment. Based on a number of previous studies, mostly carried out using OCs growing on a variety of surfaces (Anderegg et al., 2011; Destaing et al., 2003; Geblinger et al., 2009; Georgess et al., 2014), it was established that the SZ is a dynamic structure, the integrity of which depends on the assembly of its structural building blocks—namely, podosomes—into a coherent adhesive and F-actin-rich belt, and the long-term stability of this structure. The importance of SZ stability is broadly recognized; yet the underlying mechanisms remain poorly defined.

In this study, we directly monitored SZL integrity and dynamics, using fluorescent light microscopy of live, cultured OCs expressing GFP-tagged actin. In doing so, we addressed the following questions: Is the stability of the SZL regulated globally, or is it a local process, affecting only segments? How is SZL remodeling synchronized? Is the stability regulated by the modulation of actin polymerization and networking, and are other cytoskeletal systems involved in the process?

Combining live-cell dynamic monitoring and fixed-cell structural examination, we found that the stability of the SZL is structurally recognizable, in specific segments of the structure. Specifically, we identified two main modes of SZL remodeling, the first being translocations of coherent SZL or regions, and the second, characterized by loss of SZL coherence. The former process typically occurs at the cell periphery, and is seen in small SZ rings on bone. The latter is commonly observed on glass slides with fast dynamics, and was studied here.

Focusing on SZL disintegration, we noticed that concave regions along the SZL belt are considerably more likely to undergo loss of compact podosome packing and their subsequent dispersion, while convex areas seem more stable. The reason why concave SZL domains are unstable is still unclear. A possible explanation for that phenomenon may arise out of the notion that tension applied to integrin-based adhesions stabilizes the structure and stimulates its growth (Balaban et al., 2001; Geiger, Spatz, & Bershadsky, 2009; Riveline et al., 2001). It is conceivable that actin fibers bridging between podosome cores can support tension forces along the SZL: actin fibers, which emerge from the core bundle and attach to plaque proteins, can transmit these forces to the adhesion plaque (Anderegg et al., 2011). Furthermore, previous studies demonstrated that the mechanical coherence of the SZ is robust, enabling it to extend across local topographical barriers (Geblinger, Zink, Spencer, Addadi, & Geiger, 2011).

Another mechanism that may underlie the instability of concave regions might be due to lower podosome density in SZL regions of high curvature. If actin cross-bridges between podosomes are tighter at the outer (longer) side of convex SZL segments, they may temporarily relax when these segments become concave, enabling podosomes to move further apart. Tension may redevelop when convex SZL segments reassemble. This finding is compatible with SZL stable/unstable cycles. Alternative explanations would relate local regulation to the inhomogeneity of the adhesive surface, less likely in the case of OCs cultured on glass, but potentially relevant to cells adhering to bone, which overall, display similar behavior (Shemesh, Addadi, Milstein, Geiger, & Addadi, 2016); or to internal cytoskeletal regulation, which could, in principle, act either downstream or upstream of SZL concavity. While the present findings unequivocally demonstrate that SZL instability is primarily a local phenomenon, affecting concave segments rather than the entire structure simultaneously, we have no evidence that SZL geometry *per se* directly induces instability.

Interestingly, the results presented here suggest that the MT system; in particular, the podosome effector and MT-associated protein dynamin2, play a key role in regulating SZL stability. Perturbation of SZL compaction and stability by the MT-disrupting drug nocodazole was reported a decade ago (Jurdic et al., 2006) and further characterized here. Apparently, the MT system confines podosome assembly to the SZL, and its proximity. This finding, in turn, is supported by the observation that disruption of MTs not only destabilizes the SZL, but also enables podosome assembly at the cell center, away from the SZL. This apparent "regional confinement" of the two cytoskeletal systems could be attributed either to their physical coherence, or to the presence of diffusible components associated with or transported by MTs, which affect podosome assembly and/or SZL stability. We showed here that MT ends are abundant near stable and compact SZL regions, while unstable SZL segments are typically "invaded" by radially extending MTs.

While we have no direct evidence that the penetration of MTs into the SZL domain has a direct destabilizing effect, we were intrigued by the fact that both MT disruption (by nocodazole) and peripheral extension of intact MTs induced instability, and searched for MT-associated molecules that might mediate the destabilizing effect. We chose to examine the effect of dynamin2, an actin-regulating factor that affects podosome dynamics (Bruzzaniti et al., 2005; Destaing et al., 2013; McNiven et al., 2004; Ochoa et al., 2000) and bone resorption activity (Bruzzaniti et al., 2005; Tanabe & Takei, 2009). Although the majority of studies implicate dynamin in endocytosis, evidence exists to suggest that this GTPase may play additional roles in cell physiology. Dynamin2 is also associated with MTs (Maeda, Nakata,

Noda, Sato-Yoshitake, & Hirokawa, 1992), affecting the frequency of dynamic instability events (Tanabe & Takei, 2009), which was later found to control podosome patterning in OCs through EB1, cortactin, and src (Duplan et al., 2014).

During the past decade, increasing evidence indicates that dynamin2 also participates in actin control of podosomes. Notably, we found, as did others, (McNiven et al., 2004; Ochoa et al., 2000) that dynamin is associated with membrane invaginations under the center of the actin core in podosomes. The assumption is that dynamin2 is one of the cloud proteins that, through interactions with src and cbl (Bruzzaniti et al., 2005), Pyk2 (Bruzzaniti et al., 2009), and cortactin (Schafer et al., 2002), modulates actin polymerization and podosome function.

Our examination of immune-labeled OCs indicates that dynamin2 labeling is prominent along MTs, and displays diffuse but consistent labeling intensity around the SZL. Perturbation studies showed that mutations in functional domains of dynamin2, as well as its siRNA, affect SZL stability, with no apparent effect on the MTs. Inhibition of dynamin2's GTPase activity by the drug Dyngo4-a caused a phenotype similar to that recorded following MT disruption; namely, loss of SZL compaction, and dispersion of podosomes toward the cell center. This may imply that dynamin acts downstream of MTs, plausibly transported by them toward the SZL.

The fact that dynamin activity has no apparent effect on the assembly and dynamics of individual podosomes, but dramatically affects the stability of the SZL, suggests that the main function of this protein in these cells is related to podosome clustering and compaction in the SZ, probably mediated by interactions of the actin "cloud" interconnecting podosome cores.

Taken together, these results provide insights into the structure and dynamics of the SZL, demonstrate that assembly of podosomes into the SZL involve MTs, and suggest that dynamin2 is instrumental in regulating SZL stability at the cell periphery.

4 | MATERIALS AND METHODS

1. Cell cultures: A RAW 264.7 murine macrophage cell line, with or without stable transfection with GFP-actin, was cultured in α-MEM supplemented with 1% pen-strep, 1% glutamine, and 10% FCS. To induce OC differentiation, 20 ng/mL of M-CSF and 20 ng/mL of RANKL (R&D Systems, Minneapolis, MN) were added and replenished every 24 hr, for at least 3 days.
2. Immunofluorescence microscopy and time-lapse movies: Cells were plated on 35 mm glass-bottomed Petri dishes (part # P35G-0-14-C, MatTek, Ashland, MA). Images were acquired by DeltaVision model RT or Elite microscopes (Applied Precision GE, Issaquah, WA), using 100×/1.3 or 40×/1.43 oil objectives (Olympus, Hamburg, Germany). For time-lapse movies, the system was equipped with a temperature- and CO2-controlled environmental chamber.
3. Image analysis: Image analysis was performed using the UCSF Priism environment (http://msg.ucsf.edu/ive), and quantitative analysis software developed in-house. Z-stacks were deconvoluted by DeltaVision software (Applied Precision) and visualized by Imaris software (http://www.bitplane.com/go/products/imaris).
4. Transfections: Cells were transfected using Lipofectamine2000 (Invitrogen, Grand Island, NY) according to the manufacturer's instructions. Cells were cultured for 24-36 hr in complete medium on glass-bottomed plates (MatTek), then either fixed and labeled, or subjected to live-cell video microscopy.
   Plasmid encoding Ensconsin-mCherry for MT labeling (EMTB-mCherry; Addgene plasmid # 26742) was a gift of William Bement [ref: Miller AL, Bement WM. 2009. Nat Cell Biol. 11:71-7].
5. Dynamin constructs (Dynamin-2aa, dynamin-ΔPRD, dynamin-k44a) were kindly provided by the lab of Prof. Pietro De Camilli (Yale School of Medicine, New Haven, CT, USA).
6. Inhibitors: Nocodazole and Dyngo4-a were purchased from Sigma (Rehovot, Israel), dissolved in DMSO, and added to cell media at the indicated concentrations.
7. Fixation: Cells were fixed in 3% formaldehyde with 0.5% triton for 30 min. For MT labeling, 0.1% gluteraldehyde was also added.
8. Immunostaining: For labeling with the first antibody, fixed cells were incubated for 40 min in the antibody solution. Cells were then washed three times for 5 min (3 × 5) with PBS, and finally incubated with the fluorescent-conjugated second antibody for 40 min, followed by repeated cell washing (3 × 5) with PBS. Antibodies used in this study included: Mouse monoclonal α-tubulin (Sigma); goat anti-mouse IgG conjugated to Alexa Fluor 488 (Invitrogen, Carlsbad, CA, USA); goat anti-mouse IgG conjugated to Cy5, and goat anti-rabbit IgG conjugated to cy3 (Jackson Immuno Research Laboratories, West Grove, PA). F-Actin was fluorescently labeled with TRITC-phalloidin (Sigma). Dynamin2 antibody was a kind gift of Dr. Mark McNiven's lab (Mayo Clinic, Rochester, MN).
9. Super-resolution microscopy: Multicolor STORM images were acquired by the SR-200 super-resolution microscope system (Vutara, Salt Lake City, UT). Freshly mixed imaging buffer at 4°C was used (Dempsey, Vaughan, Chen, Bates, & Zhuang, 2011).

Reagents used were:

- Cysteamine (MEA) #30070-10G (Sigma) - stored at 4°C
- 2-Mercaptoethanol #63689-25ML-F (Sigma) - stored at 4°C
- Glucose oxidase type seven from Aspergillius #G2133-50KU (Sigma) - stored at −20°C
- Catalase from bovine liver C40-100 mg (Sigma) - stored at −20°C
- 1M Tris pH 8.0 # 22638 500 ML (Affymetrix/USB) - stored at room temperature
- NaCl
- Glucose

Stocks:

- Buffer A: 50 mM Tris-HCl (pH 8.0) + 10 mM NaCl) - stored at room temperature

- Buffer B: 50 mM Tris-HCl (pH 8.0) + 10 mM NaCl + 10% (w/v) glucose - stored at 4°C
- 1 M MEA: 77 mg MEA dissolved in 1 mL Buffer A - stored at 4°C
- Gloxy: glucose oxidase (Gluox) + catalase mixture dissolved in buffer A - stored at 4°C

Typical concentration: 20 mM MEA + 1% (v/v) 2-Mercaptoethanol + 1x Gloxy in buffer B.

ACKNOWLEDGMENTS

The authors would like to thank Dr. Mark McNiven for dynamin2 antibodies, and Prof. Pietro De Camilli for dynamin2 mutant RNA constructs. They are indebted to Dr. Tali Dadosh for her expert help in super-resolution microscopy. The research leading to these results was funded from the European Union's Seventh Framework Programme (FP7/2007-2013) under grant agreement n°258068, EU-FP7-Systems Microscopy NoE.

REFERENCES

Anderegg, F., Geblinger, D., Horvath, P., Charnley, M., Textor, M., Addadi, L., & Geiger, B. (2011). Substrate adhesion regulates sealing zone architecture and dynamics in cultured osteoclasts. *PLoS One*, *6*, e28583.

Balaban, N. Q., Schwarz, U. S., Riveline, D., Goichberg, P., Tzur, G., Sabanay, I., ... Geiger, B. (2001). Force and focal adhesion assembly: A dose relationship studied using elastic micropatterned substrates. *Nature Cell Biology*, *3*, 466–472.

Boyce, B. F. (2013). Advances in the regulation of osteoclasts and osteoclast functions. *Journal of Dental Research*, *92*, 860–867.

Bruzzaniti, A., Neff, L., Sanjay, A., Horne, W. C., De Camilli, P., & Baron, R. (2005). Dynamin forms a Src kinase-sensitive complex with Cbl and regulates podosomes and osteoclasts activity. *Molecular Biology of the Cell*, *16*, 3301–3313.

Bruzzaniti, A., Neff, L., Sandoval, A., Du, L., Horne, W. C., & Baron, R. (2009). Dynamin reduces Pyk2 Y402 phosphorylation and SRC binding in osteoclasts. *Molecular and Cellular Biology*, *29*, 3644–3656.

Bulinski, J. C., Odde, D. J., Howell, B. J., Salmon, T. D., & Waterman-Storer, C. M. (2001). Rapid dynamics of the microtubule binding of ensconsin in vivo. *Journal of Cell Science*, *114*, 3885–3897.

Dempsey, G. T., Vaughan, J. C., Chen, K. H., Bates, M., & Zhuang, X. (2011). Evaluation of fluorophores for optimal performance in localization-based super-resolution imaging. *Nature Methods*, *8*, 1027–1036.

Destaing, O., Ferguson, S. M., Grichine, A., Oddou, C., De Camilli, P., Albiges-Rizo, C., & Baron, R. (2013). Essential function of dynamin in the invasive properties and actin architecture of v-Src induced podosomes/invadosomes. *PLoS One*, *8*, e77956.

Destaing, O., Petropoulos, C., & Albiges-Rizo, C. (2014). Coupling between acto-adhesive machinery and ECM degradation in invadosomes. *Cell Adhesion and Migration*, *8*, 256–262.

Destaing, O., Saltel, F., Géminard, J. C., Jurdic, P., & Bard, F. (2003). Podosomes display actin turnover and dynamic self-organization in osteoclasts expressing actin-green fluorescent protein. *Molecular Biology of the Cell*, *14*, 407–416.

Destaing, O., Saltel, F., Gilquin, B., Chabadel, A., Khochbin, S., Ory, S., & Jurdic, P. (2005). A novel Rho-mDia2-HDAC6 pathway controls podosome patterning through microtubule acetylation in osteoclasts. *Journal of Cell Science*, *118*, 2901–2911.

Duplan, B. M., Zalli, D., Stephens, S., Zenger, S., Neff, L., Oelkers, J. M., ... Baron, R. (2014). Microtubule dynamic instability controls podosome patterning in osteoclasts through EB1, cortactin, and Src. *Molecular and Cellular Biology*, *34*, 16–29.

Evans, J. G., Correia, I., Krasavina, O., Watson, N., & Matsudaira, P. (2003). Macrophage podosomes assemble at the leading lamella by growth and fragmentation. *Journal of Cell Biology*, *161*, 697–705.

Geblinger, D., Geiger, B., & Addadi, L. (2009). Surface-induced regulation of podosome organization and dynamics in cultured osteoclasts. *ChemBioChem*, *10*, 158–165.

Geblinger, D., Zink, C., Spencer, N. D., Addadi, L., & Geiger, B. (2011). Effects of surface microtopography on the assembly of the osteoclast resorption apparatus. *Journal of the Royal Society Interface*, *9*, 1599–1608.

Geiger, B., Spatz, J. P., & Bershadsky, A. D. (2009). Environmental sensing through focal adhesions. *Nature Reviews. Molecular Cell Biology*, *10*, 21–33.

Georgess, D., Machuca-Gayet, I., Blangy, A., & Jurdic, P. (2014). Podosome organization drives osteoclast-mediated bone resorption. *Cell Adhesion & Migration*, *8*, 191–204.

Hagel-Bradway, S., & Dziak, R. (1989). Regulation of bone cell metabolism. *Journal of Oral Pathology and Medicine*, *18*, 344–351.

Jurdic, P., Saltel, F., Chabadel, A., & Destaing, O. (2006). Podosome and sealing zone: Specificity of the osteoclast model. *European Journal of Cell Biology*, *85*, 195–202.

Kaverina, I., Krylyshkina, O., & Small, J. V. (1999). Microtubule targeting of substrate contacts promotes their relaxation and dissociation. *Journal of Cell Biology*, *146*, 1033–1044.

Kopp, P., Lammers, R., Aepfelbacher, M., Woehlke, G., Rudel, T., Machuy, N., ... Linder, S. (2006). The kinesin KIF1C and microtubule plus ends regulate podosome dynamics in macrophages. *Molecular Biology of the Cell*, *17*, 2811–2823.

Lakkakorpi, P. T., Helfrich, M. H., Horton, M. A., & Väänänen, H. K. (1993). Spatial organization of microfilaments and vitronectin receptor, alpha v beta 3, in osteoclasts. A study using confocal laser scanning microscopy. *Journal of Cell Science*, *104*, 663–670.

Lakkakorpi, P. T., & Väänänen, H. K. (1996). Cytoskeletal changes in osteoclasts during the resorption cycle. *Microscopy Research and Technique*, *33*, 171–181.

Luxenburg, C., Addadi, L., & Geiger, B. (2006). The molecular dynamics of osteoclast adhesions. *European Journal of Cell Biology*, *5*, 203–211.

Luxenburg, C., Winograd-Katz, S., Addadi, L., & Geiger, B. (2012). Involvement of actin polymerization in podosome dynamics. *Journal of Cell Science*, *125*, 1666–1672.

Maeda, K., Nakata, T., Noda, Y., Sato-Yoshitake, R., & Hirokawa, N. (1992). Interaction of dynamin with microtubules: Its structure and GTPase activity investigated by using highly purified dynamin. *Molecular Biology of the Cell*, *3*, 1181–1194.

Manolagas, S. C. (2000). Birth and death of bone cells: Basic regulatory mechanisms and implications for the pathogenesis and treatment of osteoporosis. *Endocrine Reviews*, *21*, 115–137.

Marks, S. C., Jr. (1987). Osteopetrosis–Multiple pathways for the interception of osteoclast function. *Applied Pathology*, *5*, 172–183.

McCluskey, A., Daniel, J. A., Hadzic, G., Chau, N., Clayton, E. L., Mariana, A., ... Robinson, P. J. (2013). Building a better dynasore: The dyngo compounds potently inhibit dynamin and endocytosis. *Traffic*, *14*, 1272–1289.

McNiven, M. A., Baldassarre, M., & Buccione, R. (2004). The role of dynamin in the assembly and function of podosomes and invadopodia. *Frontiers in Bioscience*, *9*, 1944–1953.

Mulari, M., Vaaraniemi, J., & Väänänen, H. K. (2003). Intracellular membrane trafficking in bone resorbing osteoclasts. *Microscopy Research and Technique*, *61*, 496–503.

Ochoa, G. C., Slepnev, V. I., Neff, L., Ringstad, N., Takei, K., Daniell, L., . . ., De Camilli, P. (2000). A functional link between dynamin and the actin cytoskeleton at podosomes. *Journal of Cell Biology*, *150*, 377–389.

Pfaff, M., & Jurdic, P. (2001). Podosomes in osteoclast-like cells: Structural analysis and cooperative roles of paxillin, proline-rich tyrosine kinase 2 (Pyk2) and integrin alphaVbeta3. *Journal of Cell Science*, *114*, 2775–2786.

Riveline, D., Zamir, E., Balaban, N. Q., Schwarz, U. S., Ishizaki, T., Narumiya, S., . . ., Bershadsky, A. D. (2001). Focal contacts as mechanosensors: Externally applied local mechanical force induces growth of focal contacts by an mDia1-dependent and ROCK-independent mechanism. *Journal of Cell Biology*, *153*, 1175–1186.

Salter, F., Destaing, O., Bard, F., Eichert, D., & Jurdic, P. (2004). Apatite-mediated actin dynamics in resorbing osteoclasts. *Molecular Biology of the Cell*, *15*, 5231–5241.

Schafer, D. A., Weed, S. A., Binns, D., Karginov, A. V., Parsons, J. T., & Cooper, J. A. (2002). Dynamin2 and cortactin regulate actin assembly and filament organization. *Current Biology*, *12*, 1852–1857.

Shemesh, M., Addadi, S., Milstein, Y., Geiger, B., & Addadi, L. (2016). Study of osteoclast adhesion to cortical bone surfaces: A correlative microscopy approach for concomitant imaging of cellular dynamics and surface modification. *ACS Applied Material Interfaces*, *8*, 14932–14943.

Soysa, N. S., Alles, N., Aoki, K., & Ohya, K. (2012). Osteoclast formation and differentiation: An overview. *Journal of Medical and Dental Sciences*, *8*, 65–74.

Tanabe, K., & Takei, K. (2009). Dynamic instability of microtubules requires dynamin 2 and is impaired in a Charcot-Marie-Tooth mutant. *Journal of Cell Biology*, *185*, 939–948.

Teitelbaum, S. L. (2011). The osteoclast and its unique cytoskeleton. *Annals of the New York Academy of Sciences*, *1240*, 14–17.

Väänänen, H. K., & Horton, M. (1995). The osteoclast clear zone is a specialized cell-extracellular matrix adhesion structure. *Journal of Cell Science*, *108*, 2729–2732.

Väänänen, H. K., Zhao, H., Mulari, M., & Halleen, J. M. (2000). The cell biology of osteoclast function. *Journal of Cell Science*, *113*, 377–381.

SUPPORTING INFORMATION

Additional Supporting Information may be found online in the supporting information tab for this article.

MOVIE S1 Dynamics of actin and microtubules. Time-lapse movie of GFP-actinexpressing osteoclasts, further transfected with Ensconsin-mCherry to label live microtubules. Two cycles of SZL compaction and dispersion are shown (podosomes indicated by green dots), and are clearly correlated with waves of advancing and retracting microtubule ends. TT=30 seconds. TT is too long to determine if MTs or actin lead the changes. Scale bar: 25 μm

FIGURE S2 Mutant dynamins affect their localization and SZL stability. Three different plasmids of dynamin were overexpressed in osteoclasts: (A) Dynamin-2aa; SZL is normal. (B) Dynamin-TPRD; SZL is fragmented, and dynamin binding is seen around but not on the SZL; and (C) Dynamin-k44a; osteoclast fusion seems to be disrupted, resulting in small cells. Cells were fixed and stained for actin and MT. At least 20 cells that registered positive for the transfection were recorded. Scale bar: 25 μm

FIGURE S3 Suppression of dynamin2 expression inhibits podosome compaction in the SZL. Dynamin2 siRNA was transfected to osteoclasts 60 h after initiation of cell fusion. Cells were fixed and stained for: (A) Actin; (B) Dynamin2; (C) MT; and (D) DAPI, 34 hours post-transfection with siRNA. The large osteoclast at the center of the image underwent partial silencing of dynamin2, compared to its full expression in neighboring cells, as antibody staining indicates in (B). In this cell, dispersion of podosomes and uncompacted SZLs are seen, compared to the well-defined SZLs surrounding it; see (A). The MTs in (C) do not seem to be affected by the transfection. (E-H) Corresponding images of an osteoclast transfected with siGLO RNAi control (Dharmacon, Lafayette, CO, USA). Scale bar: 25 μm

How to cite this article: Batsir S, Geiger B, and Kam Z. Dynamics of the sealing zone in cultured osteoclasts. *Cytoskeleton*. 2017;74:72–81. doi:10.1002/cm.21350.